JOURNAL OF SOLID STATE CHEMISTRY **136,** 160–166 (1998)
ARTICLE NO. SC977664

Single-Crystal Studies of the Chevrel-Phase Superconductor $La_xMo_6Se_8$

II: Physical and Superconducting Properties

O. Peña,[1] F. Le Berre,[2] J. Padiou, and T. Marchand

Chimie du Solide et Inorganique Moléculaire, UMR CNRS 6511, Université de Rennes I, 35042 Rennes Cedex, France

and

R. Horyń and A. Wojakowski

Institute of Low Temperature and Structure Research, Polish Academy of Sciences, 50 950 Wroclaw 2, Poland

Received October 9, 1996; in revised form October 9, 1997; accepted October 14, 1997

Single crystals of $La_xMo_6Se_8$ have been grown and some of their magnetic, transport, and superconducting properties studied. The electrical resistivity is characterized by its high value at room temperature, its low residual resistivity ratio, and a pronounced negative curvature at high temperatures. Comparison with the isostructural compounds Mo_3Se_4 (Mo_6Se_8) and $LaMo_6S_8$ shows that this behavior is due to structural as well as to extrinsic features (e.g., brittleness due to weak intercluster bondings). The position of the Fermi level near a peak of the density of states plays an important role in the normal-state physical properties, fixing the functional forms of both resistivity and magnetic susceptibility. The superconducting state is mainly characterized by a strong lanthanum concentration dependence of the critical temperature T_c, by quite definite granular effects, and by a very high critical field ($H_{c2}(0) \sim 55$ T). The intragrain critical current density, as estimated by magnetic mesurements, is relatively high (4×10^4 A/cm^2 at zero field and 1.7 K), three times larger than the one obtained for the void compound Mo_3Se_4. This fact is due to a higher density of pinning centers in the ternary compound because of microstructural features such as microcracks or crystal defects caused by the extreme brittleness of the crystals.

1. INTRODUCTION

The rare-earth molybdenum chalcogenides of formula $REMo_6X_8$ ($X = S, Se$), discovered by Chevrel and coworkers (1–3), have been thoroughly studied. One of the main interests in these compounds is that superconductivity is not destroyed by the presence of a magnetically ordered rare-earth sublattice, leading to unusual phenomena of coexistence between magnetism and superconductivity (4–6).

Our program of research has dealt mainly with the crystal growth of the rare-earth-based Chevrel phases of the sulfide series $REMo_6S_8$. Mechanisms of growth of such series are now well understood, and they are thoroughly described in ref 7. The physical properties of such single crystals are also reviewed in refs 7 and 8. The situation in the selenide series $REMo_6Se_8$ is by far much more complicated and many questions still exist about, for instance, intrinsic magnetic properties of these phases [e.g., description of the ordered state (8)], the lack of superconductivity in some representatives [e.g., $EuMo_6Se_8$ (9, 10), and $YbMo_6Se_8$ (11)], and the probable coexistence of ferromagnetism and superconductivity [e.g., $HoMo_6Se_8$ (12)]. In addition, the critical temperature T_c of heavy rare-earth molybdenum selenides (RE: Gd → Lu) happens to be strikingly similar to the value observed in the binary Mo_3Se_4; this latter compound, which occurs very often as an impurity phase, may then hide the intrinsic properties of the ternary-phase materials.

To answer several of these questions, we have recently undertaken a research program on the growth of the selenide materials. Our present approach, described in the accompanying paper (13), allowed us to obtain single-crystal specimens of several rare-earth molybdenum selenides $REMo_6Se_8$, with RE = La, Ce, Pr, Nd, Sm, and Eu (14). In this work, we have chosen to present the case of RE = La, mainly for two reasons. First, lanthanum is the largest ion among the rare-earth elements, giving rise to the largest effects in the structural variations of the series; furthermore, $LaMo_6Se_8$ presents the highest T_c among the $REMo_6Se_8$

[1]To whom correspondence should be addressed.

[2]Part of the thesis work presented by F. Le Berre at the Université de Rennes I, France, 1996. Present address: Université du Maine, 72017 Le Mans, France.

0022-4596/98 $25.00

compounds, which facilitates the measurement of its intrinsic physical properties and makes its identification much easier with respect to the secondary phase Mo_3Se_4 (T_c = 6.45 K). Second, the domain of existence of the $La_xMo_6Se_8$ phase has been exactly defined at 1200°C in one of our previous works (15), giving us a good support for the interpretation of the experimental data.

The crystal structure and the relationships between the interatomic distances, the lanthanum occupancy, and the superconducting critical temperature are thoroughly described in Part I of this work, whereas some of the main physical properties (i.e., electrical resistivity, magnetism, and superconducting behavior at zero field or under an applied external field) constitute the subject of Part II.

2. EXPERIMENTAL

When possible, measurements were performed on individual crystals (e.g., electrical resistivity and inductive transitions); otherwise, measurements needing large quantities of material because of weak signal (e.g., dc susceptibility or magnetization) had to be performed on an ensemble of specimens. However, due to the reasons evoked in Part I (i.e., a lanthanum concentration gradient along the sample), the larger the crystal being tested, the wider the superconducting transition and the lower the accuracy in the lanthanum content. Such effects, negligible in crystals chosen for structural refinement ($V \sim 10^{-2}$ mm^3), become an important obstacle in specimens used for physical measurements, which need to be at least two orders of magnitude larger.

The immediate consequence of this is the fact that the results given herein reflect concentration effects averaged within the domain of existence of the specific Chevrel phase, in our case, between $x = 0.84$ and $x = 0.94$ for RE = La (13, 15), and no direct correlation could be drawn between the lanthanum concentration and each specific physical property. On the other hand, as already pointed out, use of single crystals will give immediate access to intrinsic properties (e.g., anisotropy) of a material freed of impurity phases.

With all these warnings concerning the exact lanthanum concentration of the measured specimens, several basic physical properties of these crystals were studied. These included electrical transport, ac susceptibility, dc susceptibility, and magnetization.

The electrical resistivity was measured between 5 and 300 K by standard four-point probe techniques with indium contacts made by ultrasound soldering (geometrical factors estimated at $\pm 20\%$ accuracy); the stabilized current was maintained below 5 mA to avoid joule heating, but it was increased by at lest a factor of 50 below T_c to confirm the zero-resistance state.

Dc magnetization and susceptibility were measured in a SHE-VTS SQUID susceptometer between 2 and 300 K at different applied dc fields. A tentative H–T phase diagram was deduced from the magnetization $M(H)$ cycles performed at different temperatures within the superconducting state (H_{c1}–T) and from the superconducting transitions recorded under different applied fields (H_{c2}–T).

A home-made ac susceptometer equipped with a mutual-inductance bridge tuned at low frequency was used to measure the inductive superconducting transitions of different crystals as described in Part I; the applied ac field was maintained below the level of 1 μT to avoid grain decoupling effects.

3. RESULTS AND DISCUSSION

3.1. Normal-State Properties

3.1.1. Electrical resistivity. The electrical resistivity was measured in several specimens, giving quite reproducible results concerning their overall $\rho(T)$ behavior. The only noticeable parameter changing from one crystal to another dealt with the superconducting transition value and its width, for the reasons discussed earlier. Figure 1 shows the electrical resistivity measured on one of our best crystals (that is, one presenting the narrowest transition $\Delta T_c \sim$ 0.8 K). Its compositon, close to $La_{0.94}Mo_6Se_8$, was deduced

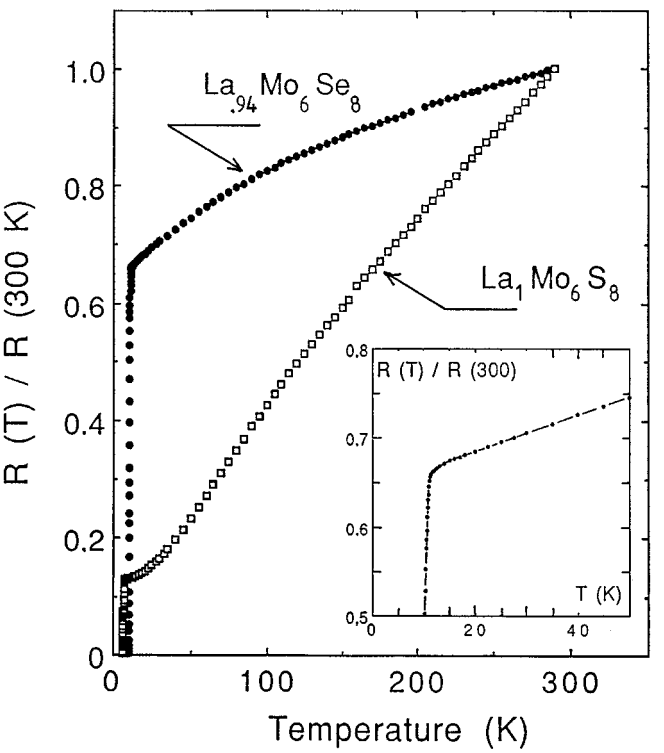

FIG. 1. Resistivity behavior of single crystals of $La_{0.94}Mo_6Se_8$ and $La_1Mo_6S_8$ (normalized to their room-temperature values, 1065 and 400 μm cm, respectively). The insert shows the low-temperature region for the $La_{0.94}Mo_6Se_8$ crystal.

from the observed critical temperature ($T_c^{onset} = 11.0$ K) using the correlation established in Part I of this work. For comparison, we also show the electrical resistivity measured in the sulfide counterpart $LaMo_6S_8$ (16), for which the chemical formula was taken as 1:6:8, in view of the arguments developed in Part I. It should be emphasized that the curves shown in Fig. 1 absolutely represent the general behavior observed for trivalent rare-earth ions in either the selenide (e.g., the case of $La_{0.94}Mo_6Se_8$) or the sulfide (e.g., the case of $La_1Mo_6S_8$) series.

Two main differences should be outlined regarding the general behaviors of selenides and sulfides: (i) the absolute value of the room-temperature resistivity ρ(300 K) and (ii) the residual resistance ratio (RRR) between the room-temperature resistance and the value observed just above the superconducting transition. In the case of $LaMo_6Se_8$ these values are, respectively, of the order of 1–2 mΩ cm for ρ(300 K) and 1–2 for RRR, values that are quite similar to those observed in single crystals of other members of the $REMo_6Se_8$ series (RE = Ce, Pr, Nd, and Sm, for instance) (14). On the other hand, typical values observed in sulfides are of the order of 500–600 μΩ cm for ρ(300 K) and about 10–20 for the resistance ratio (8) [values for ρ(300 K) as low as 50–60 μΩ cm have even been reported for $LuMo_6S_8$ (17) and $CeMo_6S_8$ (18)].

In searching for reasons for such a systematic difference, we should consider the morphology and microstructure of these materials. Intercluster distances in the selenide phases are larger than those found in the sulfide materials [for instance, 3.446 and 2.726 Å for the $(Mo–Mo)^{inter}$ and $(Mo–Se(1))^{inter}$ distances, respectively, in $La_{0.94}Mo_6Se_8$ (13) and 3.238 and 2.590 Å in $LaMo_6S_8$ (19)], implying weaker bondings in the former. As a consequence, the selenide crystals are extremely brittle and easily shatter in thin sheets, whereas sulfide crystals are much more compact, although irregular in shape. This extreme brittleness of the selenide phases brings about microcracks and crystals imperfections responsible for a high residual resistivity and a high density of pinning centers, as discussed later. At this point, we should also mention the case of the binary Mo_3Se_4, which is an exception to the aforementioned rule. This compound exhibits a lower value of ρ(300 K) (235 μΩ cm) and a RRR ratio larger than 10 (20), values that can be explained by the shorter intercluster distances [3.266 and 2.599 Å, for the $(Mo–Mo)^{inter}$ and $(Mo–Se(1))^{inter}$ distances, respectively (19)] compared to those existing in $La_{0.94}Mo_6Se_8$.

Other important differences between selenides and sulfides are readily noticeable in Fig. 1. These are connected with the functional form of the resistivity, mainly the low-temperature behavior (in the range $T_c < T \leq 50$ K) and the pronounced deviation from linearity at higher temperatures. Concerning the first point, an approximately linear temperature dependence can be observed for the $La_{0.94}Mo_6Se_8$ compound (insert, Fig. 1), whereas a power-law dependence varying approximately as αT^2 fits the behavior of the sulfide $LaMo_6S_8$ quite well. The linearity of $\rho(T)$ at low temperatures is frequently encountered in Chevrel-phase materials that present the highest critical temperatures and magnetic critical fields, of the form $M^{2+}Mo_6S_8$ (for sulfides, M = Yb, Pb, Ca, etc) or of the form $M^{3+}Mo_6Se_8$ (for selenides, M = La), that is, for nonmagnetic M ions (8). In such materials, the Fermi level is situated near a peak in the density of states (6) and its variation with temperature may explain the linear dependence of the resistivity (21). In other cases (e.g., $RE^{3+}Mo_6S_8$, example of $LaMo_6S_8$ presented in Fig. 1), the Fermi level is found near a minimum in the density of states and its thermal variation has no effect in either resistivity or magnetic susceptiblity, as we shall see later. On the other hand, the power-law αT^2 variation is more difficult to explain by a unique model, since electron–electron scattering or electron–phonon interactions, among others, may be responsible for such a dependence (22).

Concerning the deviation from linearity and saturation of the resistance at high temperatures, several models have been proposed in the case of the A-15 superconductors, any of which may equally well explain the observed behavior in the Chevrel phases (22). Among these models, the one proposed by Fisk and Webb (23), based on the interplay between the mean free path of the electrons and the crystal lattice spacing, seems to apply to the case shown in Fig. 1. These authors suggest that the saturation of the resistivity occurs because the electron mean free path cannot drop lower than the interatomic spacing in the compound, this limit being essentially determined by the crystalline structure and the lattice constant. As we discussed earlier, in our case, the intercluster distances in the selenide phases are larger than those found in the sulfide counterpart, implying a quicker saturation of the resistance.

3.1.2. Magnetic susceptibility. To perform the dc susceptibility measurements in the normal state and for the reasons mentioned in section 2, an ensemble of crystals (total weight of about of 150 mg) was selected using an optical microscope. To characterize this set of crystals, susceptibility measurements were first performed under an ac magnetic field of about 1 μT (insert, Fig. 2). The rather large width of the transition ($\Delta T_c \sim 1$ K between 10% and 90% of the transition's amplitude) is mainly due to concentration gradients and a statistical distribution of crystals whose T_c's range between 10 and 11 K. From the correlation presented in Part I, the lanthanum concentration of this group of crystals can be evaluated between $x \sim 0.87$ and $x \sim 0.95$. For simplicity, in the following such an ensemble will be referred to by its generic formulation $La_{\sim 1}Mo_6Se_8$.

The magnetic susceptibility was then measured between 5 and 300 K under an applied field of 0.5 T. The ensemble of crystals was placed inside a metallic sample holder whose

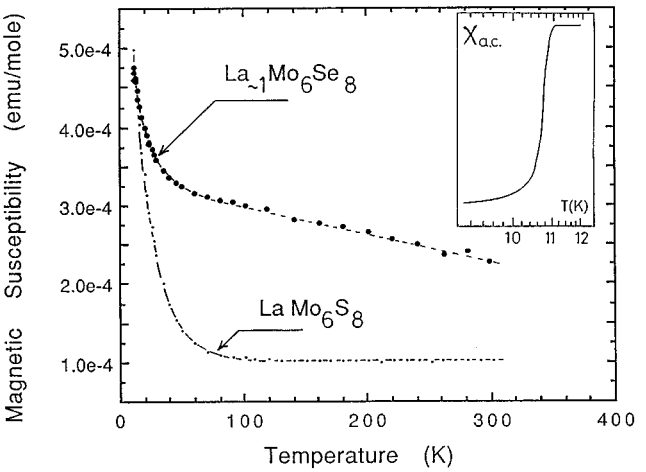

FIG. 2. Magnetic susceptiblity of two ensembles of crystals of $La_{\sim 1}Mo_6Se_8$ and $LaMo_6S_8$ measured at 0.5 T. The insert shows the inductive transition (measured under 1μT ac field) of the same ensemble of crystals of generic formulation $La_{\sim 1}Mo_6Se_8$.

magnetic signal was almost temperature independent. At each measured temperature, the sample holder's contribution (on the order of 70% of the total signal) was carefully subtracted, and the results were plotted as a function of temperature (Fig. 2). The overall behavior of the magnetic susceptibility can be described by two well-defined regions: (i) an almost linear temperature dependence in the range $50\ \text{K} \leq T \leq 300\ \text{K}$ and (ii) a small rise of the paramagnetic signal at lower temperatures. For comparison, the magnetic susceptibility of a similar set of crystals of the sulfide compound $LaMo_6S_8$, measured under identical conditions (16), is also shown in Fig. 2. The upturn at low temperatures can be ascribed to minute amounts of paramagnetic impurities present in the starting compounds (lanthanum metal for the preparation of La_2Se_3 or lanthanum oxide for La_2S_3). For instance, assuming another rare-earth element (e.g., gadolinium, $\mu = 7.94\ \mu_B$) to be responsible for such an upturn, the respective molar concentrations would be on the order of 0.05% and 0.07% for the selenide and sulfide samples.

Concerning the magnetic susceptibility at higher temperatures, it is clear from Fig. 2 that the linear thermal variation is only observed in the selenide sample $La_{\sim 1}Mo_6Se_8$ whereas the sulfide compound $LaMo_6S_8$ shows an absolutely constant behavior. The experimental values for the selenide compound (2.3×10^{-4} and 3.25×10^{-4} emu/mol at 300 and 50 K, respectively) are in excellent agreement with those reported in the literature for bulk samples (6, 24). Fischer explained this temperature dependence by the relative position of the Fermi level near a peak in the density of states (6) as it occurs in the other high critical field materials of this family. As discussed in section 3.1.1, this feature is observed in the sulfide series with divalent cations (e.g., $PbMo_6S_8$) or in the selenide series with trivalent atoms (e.g., $LaMo_6Se_8$) and constitutes a remarkable difference between $M^{2+}Mo_6S_8$ and $M^{3+}Mo_6Se_8$, on one hand, and $M^{3+}Mo_6S_8$ and $M^{2+}Mo_6Se_8$, on the other.

3.2. Superconducting Properties

3.2.1. T_c versus external magnetic field. The same set of crystals characterized in section 3.1.2 was used to investigate the magnetic field dependence of the superconducting temperature. Crystals were cooled to 4.5 K outside the superconducting coil, that is, under no magnetic field; they were then introduced into the coil and the dc field was applied. The superconducting-to-normal transitions were then recorded with increasing temperature. Values of the applied magnetic field ranged from 0 to 5 T. However, the zero-field value was not attained because of the remanent field of the coil, which depends on the history (i.e., previous applied fields) of the superconducting magnet. On the basis of our own experience and from $M(H, T)$ curves investigated under similar conditions, we can estimate this remanent field (hereafter called H_{rem}) to a maximum value of about 3×10^{-3} T, low enough compared to the fields used in this work, but very high compared to the ac magnetic field used in the inductive measurements, as we shall discuss shortly.

Figure 3 shows three superconducting transitions obtained: (a) at H_{rem}, (b) at 2 T, and (c) at 5 T. Wide transitions are observed in all cases. Three main reasons may contribute to the broadness of these transitions: first, a lanthanum concentration gradient, as discussed in section 2; second, grain decoupling, as observed in most of the high-T_c superconductors but also in Chevrel-phase materials (25); and third, a nonnegligible dependence of the critical field H_{c2} on the lanthanum concentration. If one compares the

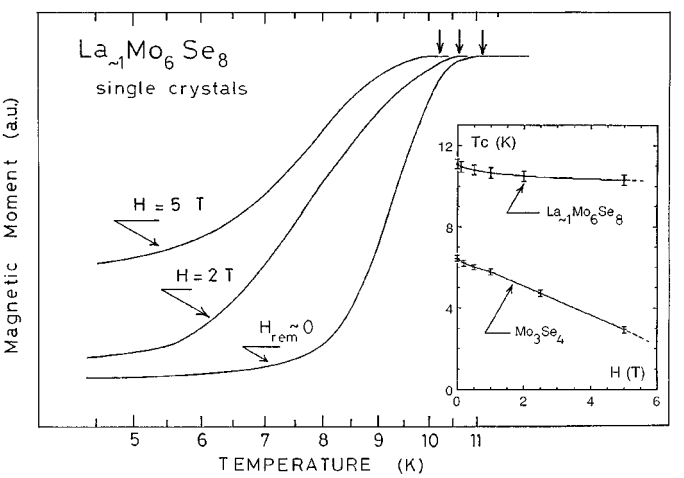

FIG. 3. Superconducting transitions of the same ensemble of crystals of $La_{\sim 1}Mo_6Se_8$ described in Fig. 2, measured under different applied dc fields. The insert shows the onset critical temperatures T_c^{onset} (marked by vertical arrows) versus field for $La_{\sim 1}Mo_6Se_8$ and Mo_3Se_4 single crystals.

transition widths observed for the same sample at very low ac field (insert, Fig. 2) and under H_{rem} (ΔT_c increases by a factor of ~ 3), it becomes evident that a most probable mechanism for broadening is granular effects, especially since brittleness may favor the existence of Josephson junctions throughout the crystals; of course, by this mechanism, the higher the applied field, the broader the transition becomes. Concerning the third hypothesis, it becomes difficult at this stage (for the reasons evoked before) to evaluate any concentration dependence of the critical field; however, similar experiments performed in the binary phase Mo_3Se_4 also showed important brodening (26) and exclude any lanthanum concentration effects on the width of the transition.

From the thermal variation of the dc moment recorded under different fields, we can draw a tentative phase diagram H_{c2}–T. The insert, of Fig. 3 shows such a phase diagram for our set of crystals of generic formulation $La_{\sim 1}Mo_6Se_8$ compared to a similar experiment performed in single crystals of the binary Mo_3Se_4 phase (20, 26). The onset temperature T_c^{onset} was defined as the departure of the magnetic moment from the normal-state zero baseline, as indicated by the vertical arrows in Fig. 3. This procedure was preferred to others (e.g., midpoint of the transition), since it reflects the intrinsic behavior of the material and does not take into account granular effects that broaden the superconducting transition. It is important to note that transitions measured by resistivity methods (narrower, as shown in the insert of Fig. 1) should give an H–T phase diagram similar to the one schematized in Fig. 3.

The onset temperature T_c^{onset} decreases very slightly in the case of the ternary phase $La_{\sim 1}Mo_6Se_8$ (from 11.1 K at zero field down to 10.3 K under 5 T), whereas a pronounced decrease is observed for the binary phase Mo_3Se_4 (from 6.45 K at zero field down to 3 K under 5 T). In the case of $La_{\sim 1}Mo_6Se_8$, the initial slope $(dH_{c2}/dT)_{T=T_c}$ is on the order of 6–7 T/K, and from this, an estimation of the critical field at zero temperature $H_{c2}(0)$ can be made by linear extrapolation of the low-field values. However, it is well known that in such extremely high critical field superconductors, a paramagnetic limit occurs because of the spin–orbit coupling (6). Under the assumption of weak coupling, H_{c2} reaches 55 T at zero temperature for single crystals of $La_{\sim 1}Mo_6Se_8$, in excellent agreement with values reported in sintered pellets (27, 28). In the case of the binary phase Mo_3Se_4, a direct extrapolation of the experimental data yields a value one order of magnitude smaller ($H_{c2}(0) \sim 8$ T) (26).

3.2.2. Magnetization and intragrain critical currents. Using the zero-field-cooled procedure described before, we performed magnetization measurements as a function of the applied field at different temperatures $T < T_c$. Figure 4 shows the magnetization half-cycle mesured at 1.7 K on the same ensemble of crystals. The behavior corresponds to an extreme type-II superconductor, with a very low critical

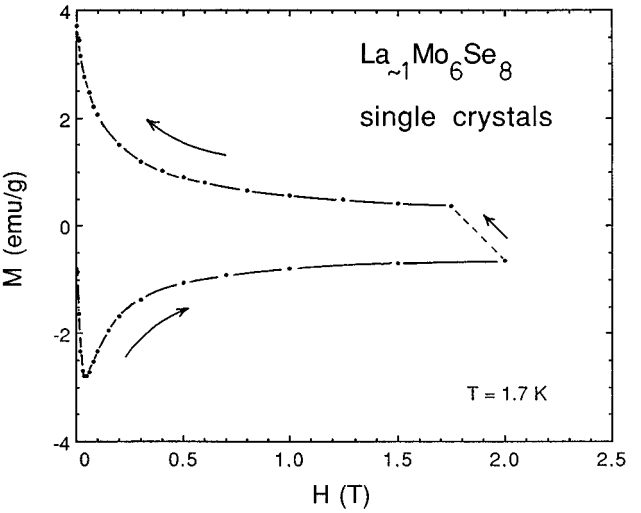

FIG. 4. Magnetization cycle measured at 1.7 K on the same ensemble of crystals of $La_{\sim 1}Mo_6Se_8$.

field H_{c1} and an extremely high H_{c2} field. The initial slopes of the magnetization curves measured under increasing fields are better seen in Fig. 5. A rough estimation of the initial susceptibility χ_{ini} (see broken lines in Fig. 5a) yields a value between -0.15 and -0.07 (emu/cm^3). These experimental slopes are overestimated because no account is taken of the remanent field of the superconducting coil (ca. 3×10^{-3} T) (29). Nevertheless, these values bracket fairly well the theoretical susceptiblity of a bulk superconductor ($\chi^{th} = -\frac{1}{4}\pi = -0.08$ emu/cm^3), without correction for the demagnetizing factor.

In a similar manner, we can estimate the critical field H_{c1}, corresponding to the point where the magnetic moment departs from the linearity of the initial susceptibility. These values, estimated between 3×10^{-3} and 6×10^{-3} T at 1.7 K (29), are of the same order as those observed in nonmagnetic Chevrel-phase superconductors (30). Since large errors are made in the experimental determination of H_{c1}, we have defined a characteristic field H_{max} (denoted by vertical arrows in Fig. 5a) for which the first branch of the magnetization ($-M(H)$) reaches a maximum. The temperature variation of H_{max} defines the H–T phase diagram depicted in Fig. 5b, which has the same form as the field dependence of the critical temperature (or H_{c2}–T plot) discussed earlier.

The intragrain critical current density J_{cg} was estimated from the static magnetization using the well-known relation $J_{cg}(\text{A/cm}^2) = 15(M^+ - M^-)/R$ (31), where M^+ and M^- are the increasing and decreasing branches of the magnetization curves (expressed in emu/cm^3) and R (in cm) is a characteristic dimension of the sample (in our case, a radius of 0.15 mm averaged over several crystals used in this experiment). Figure 6 shows the field dependence of J_{cg} at 1.7 K for our ensemble of crystals of generic formulation

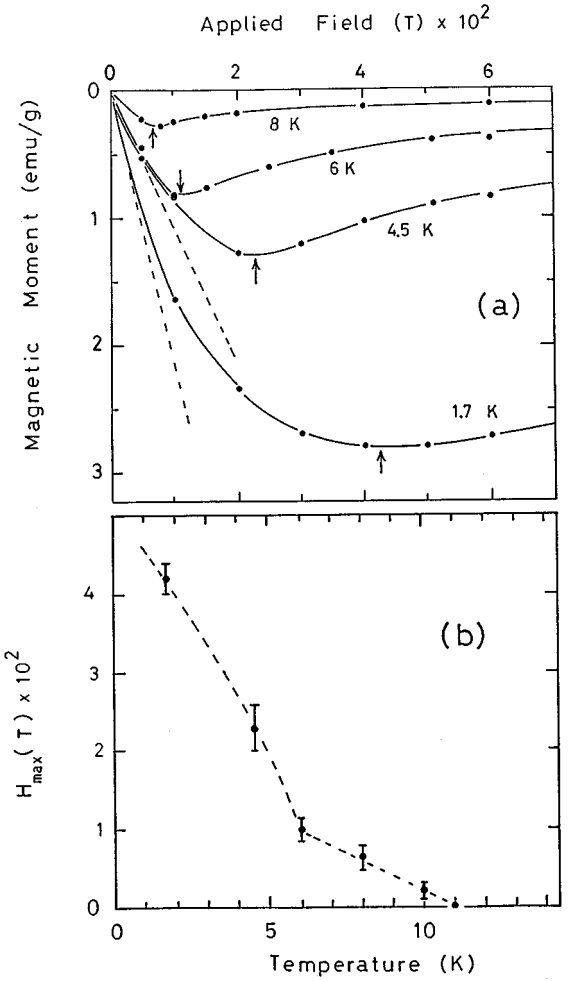

FIG. 5. (a) Low-field values of the increasing branch of the magnetization recorded at different temperatures on the same ensemble of crystals of $La_{\sim 1}Mo_6Se_8$. Vertical arrows define H_{max}, which is plotted in (b) as a function of temperature.

$La_{\sim 1}Mo_6Se_8$ compared to J_{cg} of Mo_3Se_4 estimated in a similar fashion. A rough factor of 2–3 is observed at low and intermediate fields ($H_{app} < 0.5$ T), probably due to a higher density of pinning centers. Since it is believed that such centers are connected to microscopic crystal defects, it is then possible that the stronger pinning observed in the ternary compound is closely related to its higher residual resistivity compared to that of the Mo_3Se_4 binary, as we already discussed in section 3.1.1. Obviously, the absolute values of J_{cg} should be viewed with caution since such an estimation is inversely proportional to R, which is far from being an intrinsic parameter. However, Fig. 6 gives a good qualitative confirmation that the ternary $LaMo_6Se_8$ compound is a better superconducting material than the binary compound. Direct measurements of both H_{c2} and J_{cg} by electrical resistivity techniques are planned for the near future.

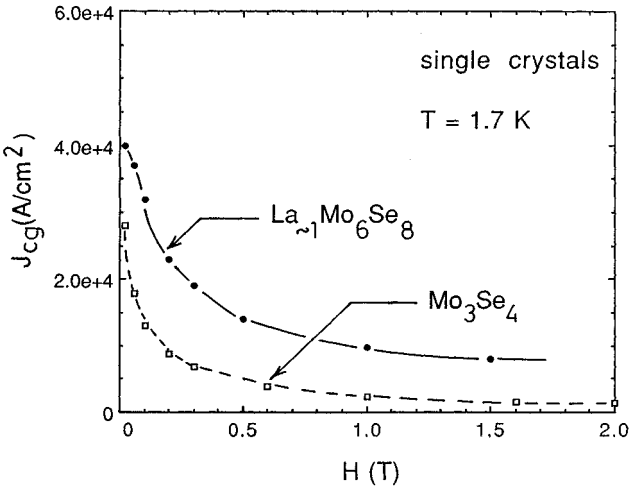

FIG. 6. Critical current densities estimated at 1.7 K using the Bean model (31) for the same ensemble of crystals of $La_{\sim 1}Mo_6Se_8$ compared to the binary Mo_3Se_4.

4. CONCLUSION

The basic physical properties of the high-T_c, high-H_{c2} superconducting material $LaMo_6Se_8$ ($T_c = 11.K$, $H_{c2}(0) \sim 55$ T) have been investigated. Results presented in the accompanying paper showed a clear dependence of T_c on the lanthanum concentration. In the present work, we show that not only structural parameters (e.g., intercluster distances) but also microstructural features (e.g., morphology and brittleness) have a direct influence on the absolute values of the electrical resistivity due to the interplay between the electron mean free path and the interatomic distances.

A direct comparison with isostructural compounds (the sulfide counterpart $LaMo_6S_8$ and the "void" phase Mo_3Se_4) allowed us to correlate the functional forms of both resistivity and magnetic susceptibility with the position of the Fermi level on the density of states (DOS). Thus, a linear variation of $\rho(T)$ at low temperatures and of $\chi(T)$ at high temperatures is observed in $LaMo_6Se_8$ because the Fermi level is situated near a peak of the DOS, whereas an αT^2 dependence of the resistivity and quite constant susceptibilities are observed in $LaMo_6S_8$ and Mo_3Se_4, for which the Fermi level is situated near a minimum of the DOS.

Microstructure plays an important role in the superconducting properties since it favors the existence of Josephson junctions and enhances the density of pinning centers in our crystals. These effects are observed through an intrinsic broadening of the superconducting transition and by a higher critical current density than in the binary compound.

Due to the growth mechanisms described in Part I, crystals used in most of our measurements showed a gradient in the lanthanum concentration. As a consequence, a direct correlation between some physical properties with the lanthanum content is difficult to establish when using an

ensemble of crystals. The superconducting parameters that we obtained under these conditions (H_{c2} estimated to about 55 T at zero temperature, and H_{c1} of the order of a few millitesla) confirm previous results obtained in sintered pellets. However, the use of single crystals allowed us to present unambiguously the intrinsic properties of this material, and future work will be devoted to the study of anisotropic effects, mainly in systems containing magnetic ions instead of nonmagnetic lanthanum.

REFERENCES

1. R. Chevrel, M. Sergent, and J. Prigent, *J. Solid State Chem.* **3,** 515 (1971).
2. M. Sergent and R. Chevrel, *J. Solid State Chem.* **6,** 433 (1973).
3. R. Chevrel, M. Sergent, and J. Prigent, *Mater Res. Bull.* **9,** 1487 (1974).
4. Ø. Fischer, A. Treyvaud, R. Chevrel, and M. Sergent, *Solid State Commun.* **17,** 721 (1975).
5. R. N. Shelton, R. W. McCallum, and H. Adrian, *Phys. Lett. A* **56,** 213 (1976).
6. Ø. Fischer, *Apply. Phys.* **16,** 1 (1978).
7. R. Horyń, O. Peña, C. Geantet, and M. Sergent, *Supercond. Sci. Technol.* **2,** 71 (1989).
8. O. Peña and M. Sergent, *Prog. Solid State Chem.* **19,** 165 (1989).
9. C. Rossel, H. W. Meul, A. Junod, R. Baillif, Ø. Fischer, and M. Decroux, *Solid State Commun.* **48,** 431 (1983).
10. C. W. Chu, S. Z. Huang, C. H. Lin, R. L. Meng, M. K. Wu, and P. H. Schmidt, *Phys. Rev. Lett.* **46,** 276 (1981).
11. J. M. Tarascon, D. C. Johnson, and M. J. Sienko, *Inorg. Chem.* **21,** 1505 (1982).
12. J. W. Lynn, J. A. Gotaas, R. W. Erwin, R. A. Ferrell, J. K. Bhattacharjee, R. N. Shelton, and P. Klavins, *Phys. Rev. Lett.* **52,** 133 (1984).
13. F. Le Berre, O. Peña, C. Perrin, M. Sergent, R. Horyń, and A. Wojakowski, *J. Solid State Chem.* **136,** 151 (1998).
14. F. Le Berre, O. Peña, C. Hamard, R. Horyń, and A. Wojakowski, *J. Alloys Compd.*, in press.
15. F. Le Berre, O. Peña, M. Sergent, R. Horyń, and A. Wojakowski, Vth Eur. Conf. on Solid State Chem., Montpellier, France, Sept. 4–7 1995; R. Horyń, F. Le Berre, A. Wojakowski, and O. Peña, *Supercond. Sci. Technol.* **9,** 1081 (1996).
16. T. Marchand and O. Peña, Internal Report, Université de Rennes I, 1996.
17. C. Geantet, R. Horyń, J. Padiou, O. Peña, and M. Sergent, *Physica B* **163,** 431 (1990).
18. O. Peña, C. Geantet, R. Horyń, M. Potel, J. Padiou, and M. Sergent, *Mater. Res. Bull.* **22,** 109 (1987).
19. K. Yvon, *in* "Current Topics in Materials Science" (E. Kaldis, Ed.), Vol. 3, pp. 53–129. North-Holland, Amsterdam 1979.
20. F. Le Berre, Thesis, University of Rennes, 1996.
21. R. W. Cohen, G. D. Cody, and J. J. Halloran, *Phys. Rev. Lett.* **19,** 840 (1967).
22. R. A. Martin and L. R. Corruccini, *J. Low Temp. Phys.* **55,** 527 (1984); R. A. Martin, Ph.D Thesis, University of California at Davis, 1981.
23. Z. Fisk and G. W. Webb, *Phys. Rev. Lett.* **36,** 1084 (1976).
24. D. C. Johnston and R. N. Shelton, *J. Low Temp. Phys.* **26,** 561 (1977).
25. D. Cattani, J. Cors, M. Decroux, and Ø. Fischer, *IEEE Trans. Magn.* **27,** 950 (1991).
26. F. Le Berre, D. Tshimanga, A.-L. Guilloux, J. Leclercq, M. Sergent, O. Peña, R. Horyń, and A. Wojakowski, *Physica B* **228,** 261 (1996).
27. S. Foner, E. J. McNiff, Jr., R. N. Shelton, R. W. McCallum, and M.B. Maple, *Phys. Lett. A* **57,** 345 (1976).
28. Ø. Fischer, M. Decroux, M. Sergent, and R. Chevrel, *J. Phys., Colloq.* **39,** C2-257 (1978).
29. The latest measurements were performed at 1.7 K in a single crystal ($T_c^{onset} = 11.0$ K, $\Delta T_c \sim 1$ K) using a Quantum Design susceptometer ($H_{rem} < 5 \times 10^{-4}$ T). Experimental values fully agree with those presented in the text: $\chi_{ini} = -0.09(1)$ emu/cm^3 and $H_{c1} \sim 5(1) \times 10^{-3}$ T.
30. C. Geantet, J. Padiou, O. Peña, M. Sergent and R. Horyń, *Solid State Commun.* **64,** 1363 (1987).
31. C. P. Bean, *Phys. Rev. Lett.* **8,** 250 (1962).